Paper ID ICLASS06-083
THE INFLUENCE OF SURFACTANTS ON IMPACTING DROPS

Aleksey Rozhkov [1], Bernard Prunet-Foch [2] and Michèle Vignes-Adler [3]

[1]Institute for Problems in Mechanics, Russian Academy of Sciences, Moscow (Russia) rozhkov@ipmnet.ru
[2]LPMDI, University of Marne la Vallée, UMR 8108 CNRS (France) Bernard.Prunet-Foch@univ-mlv.fr
[3]LPMDI, University of Marne la Vallée, UMR 8108 CNRS (France), Michele.Adler@univ-mlv.fr

ABSTRACT In many practical applications, the coating of solids is obtained by spraying complex liquids such as surfactant or/and polymer solutions on the surface. Upon collision with the solid, the droplets become highly deformed in the shape of a more or less flat wetting film in a few milliseconds, and then, they relax towards equilibrium. This very strong and short deformation causes the droplets to so much depart from equilibrium that the transient values of the physical properties of the liquid itself can be drastically different from the equilibrium ones. In the case of polymer solutions, elastic stresses arise from the elongation of the polymer chains, and in the case of surfactant solutions, there is no longer equilibrium between the adsorbed surfactants at the surface and those in the film core. The consequences are severe for the quality of the coating which is damaged by the excessive occurrence of splashes, of detaching satellite droplets, or of thickness irregularities. To analyze these effects, we have realized impacts of drops on disk-like targets of same size as the diameter of the impacting drop. Upon collision with these small targets, the drop is transformed into a thin lamella with free surfaces bounded by a thicker toroidal rim giving rise to splashes in a way which depends on the nature of the additives and their concentration in solution The high and fast deformation of the drop liquid with the above mentioned transient change of the physical properties similarly occurs on a small target that it does on a large plate, but the viscous interaction of the liquid with the solid surface is now suppressed. The physical situation is therefore simpler in the former, which enabled us to calculate the drop dynamics and to carefully analyze the influence of the dynamic physical properties of the surface-active solutions in a pure view. A major practical conclusion of our studies is that under very similar impact conditions, surfactants can either stabilize the lamella or destabilize it depending on their nature and their concentration in solution.

Keywords: Droplet impact, Surface-active solutions, Dynamic surface tension, Small target

1. INTRODUCTION

Most liquids in spraying processes are surfactant or polymeric solutions at different degrees. To know how drops from these liquids behave in impact processes is of utmost importance for aerosol coating, inkjet printing, agricultural spray and for any technologies where liquid droplets are impacting a substrate.

The collision of a drop with a plane unbounded solid substrate results in a very fast liquid lamella growth and a subsequent relatively slow retraction. In the case of a drop of a surface-active solution impacting a planar solid substrate of low surface energy [1-2], it was observed that surfactant additives do not influence the growth-stage, whereas they can very significantly slow the lamella retraction [3]. During the stage, the liquid in the drop experiences a high rate of bulk and surface deformations, and the subsequent drop retraction is driven by the 'response' of the liquid to these extreme circumstances. Generally speaking, a 'fresh' surface is formed very fast in comparison with the kinetics of surface adsorption of the surfactant; therefore the process is controlled by a dynamic surface tension effect. Then, the retraction stage is influenced by the ability of the surfactants to restore the equilibrium surface concentration decreasing the dynamic surface tension towards its equilibrium value.

The purpose of the present work is the understanding of the surfactant-related mechanisms that drive the lamella dynamics as well as its disintegration. To achieve this task, we have used a small target instead of a large plate. The reason for this particular experimental configuration is to remove the viscous friction caused by the drag exerted by the solid plate on the drop liquid, and to analyze the role of the surfactants in the impact process in a pure view.

2. EXPERIMENTAL

2.1 Materials

The tested liquids were aqueous solutions of dioctyl sulfosuccinate sodium salt (DOS) and of trisiloxane oxypropylene polyoxyethylene (Silwett L77). DOS was supplied by Acros Organics and Silwett L77 by Crompton Europe S.A. Milli-Q distilled water at room temperature was used as solvent in all cases. DOS molecules have two long chains and as their concentrations increase in solution, they organize as vesicles [4], while Silwett L77 molecules which have a very large polar head with only one chain form more or less spherical micelles at low concentration and then lamellar aggregates of different kinds as the concentration increases [5].

The main difference between DOS and Silwett L77 in solution at same concentration (in *cac* unit) is the following: DOS is a 'fast' surfactant, which means that the solution surface tension relaxes relatively rapidly to its equilibrium value if a 'fresh' surface is formed. On the contrary, Silwett L77 is a very effective, however a 'slow' surfactant, its surface tension relaxing relatively slowly toward equilibrium. Figure 1 illustrates these properties.
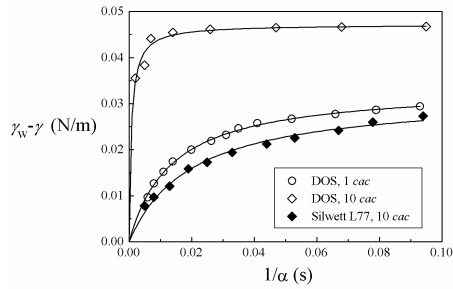
Fig. 1: Dynamic surface tension of DOS and Silwett versus the inverse of the surface dilational rate measured with the Maximum Bubble Pressure Method.

2.2 Experimental procedure

Drops were slowly generated at the tip of a capillary connected to a syringe pump in 30 – 60 seconds. This time is large enough to ensure equilibrium between the surface-active molecules in the bulk and at the surface. Drops detached from the capillary under the action of gravity, fell from a height equal to 65cm, and reached the target at velocities v_i of order of 3.4 m/s. The drop diameters d_i were in the range of 2.5 - 2.8 mm.
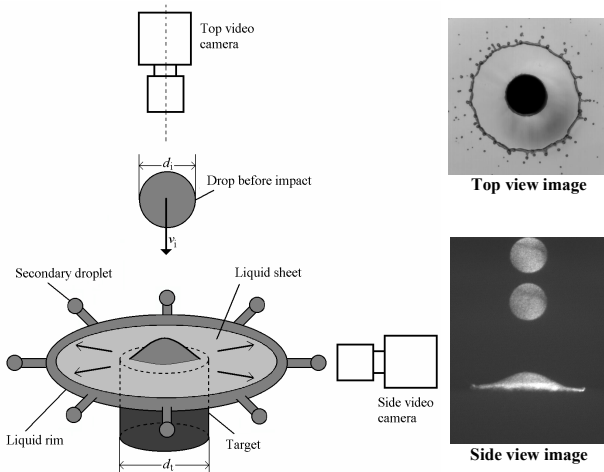
Fig. 2: Set-up and high speed visualization technique. Black circle in center of the top view image is a disk-like target of diameter 3.9 mm. Side video camera gave superimposition of two drop images before impact and one in the process impact.

Under typical conditions, d_i=2.7 mm, μ=1mPa·s, and $\gamma=\gamma_w$=72mN/m (γ_w is the water surface tension). The time scale of the process is $t_*=d_i/v_i$=0.794 ms, the impact Reynolds number ($Re=\rho v_i d_i/\mu$) is 9180, and the impact Weber number ($We=\rho v_i^2 d_i/\gamma$) is 433.

The carefully polished planar end surface of a stainless steel cylinder ($\varnothing$ = 3.90±0.05 mm) with a slightly blunt edge ($\approx$ 0.1 mm) was used as a target. The cylinder axis was aligned with the drop trajectory. Before each impact, the target surface was processed by a jet of compressed nitrogen to remove the liquid remained there from previous impacts.

We used a video recording of top views of the drop impact by means of a high speed camera equipped with a strobe lightening. The grabbing frequency was 1000 frames per second and the exposure time 1 µs. Output frames had a resolution of 1024×512 pixels with 256 grey levels.

3. RESULTS

A few examples of top view observations of impacts of surfactant solutions drops are presented in figures 3-4. Images of water drops are also given for reference. The solutions concentrations were 1×cac in figure 3, and 10×cac in figure 4. For all the solutions, the drops form a thin liquid lamella with a relatively thick toroidal rim like the water ones [6].
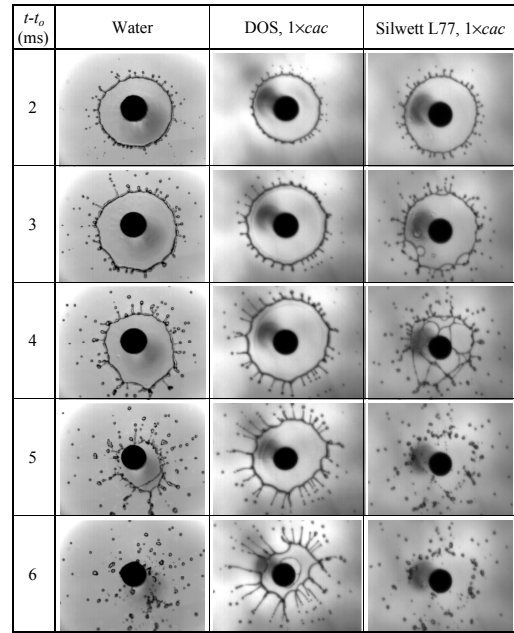
Fig. 3: Sequences of video frames depicting the collision of drops of water and of surfactant solutions at C=1×cac with a disk-like target at impact velocity of about 3.4 m/s.
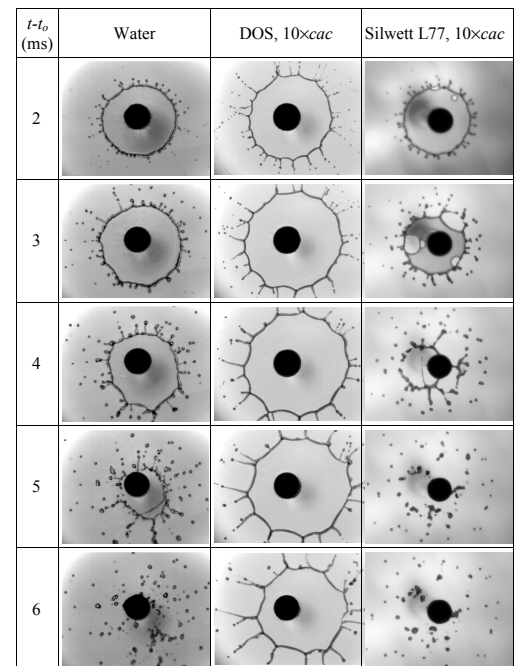
Fig. 4: Same caption as in Fig. 3 with C=10×cac

Results show that the surface-active additives can modify the impact of water drops on a small target at least in three ways.

(1) The first observable modification is a more intensive finger formation and a slight increase of the stability of the liquid fingers in comparison with the case of pure water. The most stable fingers are obtained with DOS drops. Secondary jets ejected from the rim look longer than in the case of pure water, they do not quickly disintegrate, but they transform into liquid filaments, forming a spider-like structure, like for polymer solutions [7]. However, in the case of surfactants the reason for this aspect is different from the one for polymers. The increase of the filament lifetime is not here related to inner elastic stresses in the filament as it occurred with polymer solutions, but it is caused by the decrease of the surface tension, a high value of the surface tension favouring filament disintegration.

The second modification is connected with the influence of the surfactants on the lamella spread factor. Figure 5 shows that for DOS solution at $C=1\times cac$, and for Silwett L77 solutions at $C=1$ and $10\times cac$, the spread factor $\beta=\beta(\tau)$ satisfactorily coincides with the one for pure water. In particular the maximum spread factors, β_m^w for water and β_m for these solutions can be estimated as $\beta_m^w \sim \beta_m \sim 5.0$. It means that the impacts are controlled by the dynamic surface tension, which is practically equal to the water surface tension for these solutions. Besides, figure 5 shows that the spread factor of the DOS solution at $C=10\times cac$ significantly exceeds the water spread factor as $\tau >2$, its maximum size being $\beta_m \sim 6.0$. Besides, the lifetime of the lamella becomes noticeably larger than the one of water under same impact conditions.
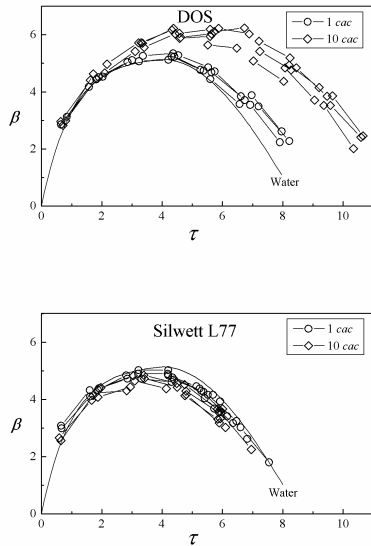
Fig. 5: Dimensionless diameter of the lamella $\beta =d/d_i$ for tested solutions, $C=1\times cac$ (circles) and $10\times cac$ (diamonds), as a function of dimensionless time $\tau =t/(d_i/v_i)$

The third modification of the lamella caused by the presence of surfactants was rather unexpected: holes spontaneously nucleated in the internal part of the lamellas of Silwett L77 solutions at $t\sim 3$ ms for the dilute solution and at $t\sim 2$ ms at $10\times cac$.

4. DISCUSSION

To analyse the effects of the surface tension changes on the lamella flow, we have modelled the lamella formation as resulting from a steady cylindrical liquid source (figure 6), of diameter d_s, supplying an axisymmetric free liquid film with initial flow rate q_s, velocity v_s, thickness h_s, liquid surface tension γ_s, and surface concentration of surfactant Γ_s at the point of ejection $r=r_s\equiv d_s/2$ like in [8]. The ejection parameters are $v_s\approx v_i$, $d_s\approx d_i$, and $\gamma_s\approx\gamma_i$.

The lamella behavior results from the continuous competition between the inertial forces that drive the drop liquid outwards (figure 6) whereas the unbalanced capillary forces acting on the lamella surfaces pull back the liquid in a thickening rim at constant velocity relatively to the film (figure 7)

$$v_r = (2\,\gamma/\rho h)^{1/2}\,, \qquad (1)$$

where γ is the liquid surface tension, ρ the liquid density and h the film thickness. The maximum extension of the lamella, r_m, is obtained when the velocity, v, of the free liquid film and the one of the rim velocity are equal, that is when the local Weber number, $We=\rho v2h/2\gamma$, is equal to 1. With a water drop, it was shown in [8] that $r_m = \rho q_s v_s/4\pi\gamma_w$ and that the thickness of the lamella close to the rim $h_m^w=q_s/(2\pi r_m^w v_s)$.
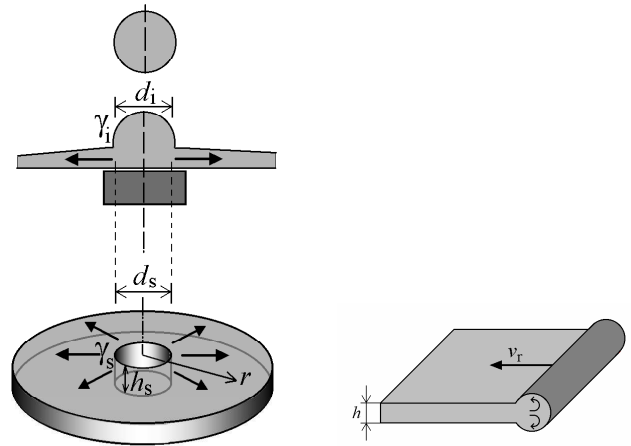
Fig. 6: Modelling of the lamella as a liquid sheet arising from radial ejection of liquid from a cylindrical source

Fig. 7: Liquid rim of a motionless liquid sheet moving with velocity $v_r=(2\gamma/\rho h)^{1/2}$

4.1. Equation of motion

Assuming that the film thickness h is small enough, in comparison to all other length scales, to use the approximation of flat velocity profile in the film, the kinematic and dynamic variables in the lamella are only function of the radial coordinate r: $v=v(r)$, $h=h(r)$.

The liquid surface tension, $\gamma=\gamma(r)$, changes under the influence of two factors. The first one is related to the residual surfactants initially adsorbed at the drop surface

before impact, whose concentration drops due to the high rate of deformation experienced by the drop surface, increasing the local surface tension in different parts of the lamella. The second factor is the surfactant flux from the bulk lamella to the surface, which tends to restore the equilibrium surfactant adsorption (figure 8).

The equation of motion follows from the momentum balance for a motionless control volume in the lamella:

$$\frac{d\left(r\rho v^2 h\right)}{dr} = 2r\frac{d\gamma}{dr} \qquad (2)$$

Introducing in (2) the continuity equation

$$q_s = 2\pi rhv, \qquad (3)$$

we obtain:

$$\frac{dv}{dr} = \frac{4\pi r}{\rho q_S}\frac{d\gamma}{dr}. \qquad (4)$$

Equation (4) represents the balance between the lamella inertia and the so-called Marangoni stresses. It shows that, in a lamella with constant surface tension, the liquid velocity does not change [6,7]. If the surface tension γ decreases as r increases, then the liquid velocity v also decreases, and vice versa.

4.2. Surfactant transfer kinetics

Surfactant mass balance is described as

$$\frac{1}{r}\frac{d\left(\Gamma v r\right)}{dr} = J, \qquad (5)$$

where Γ is the surface concentration of the free surfactant molecules (monomers). The left term in (5) describes the surfactant transfer due to the deformation of the surface, and the right one describes the flux of surfactant, J, from the bulk to the surface [9].

Assuming that the surfactant transfer is purely diffusive, the flux J is given by [10].

$$J = D\frac{\partial c}{\partial n}\bigg|_{n=0} \sim D\frac{c}{\delta}, \qquad (6)$$

where D is the diffusion coefficient, c, the bulk concentration of the free surfactant molecules (monomers), n, the normal to the surface, δ, the thickness of the diffusion boundary layer. The estimate (6) is based on the statement that due to the high rate of surface dilation, the surface concentration Γ and the subsurface bulk concentration c_{sub} are small in comparison with the saturation surface concentration Γ_∞ and the bulk concentration c, accordingly [1-3, 11].
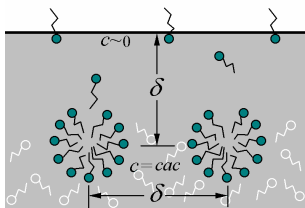
Fig. 8: Transfer of surfactant molecules from disintegrated aggregates to the almost pure surface.

The magnitudes of δ and c in (6) depend on the surfactant total concentration C. For dilute solutions, with $c=C \leq 1\times cac$, the thickness δ grows with r because of surfactant depletion in the solution in the vicinity of the surface induced by the consumption of surfactants by the dilating surface. In this case, δ scales as $rPe^{-1/2}$, where $Pe=vr/D$ is the local Péclet number [12].

For concentrated solutions with $C\gg1\times cac$, the dilution of the solution near the surface is compensated by the disintegration of aggregates, where most surfactant molecules are concentrated. In this case, the limiting step to surfactant transport is the direct diffusive transfer of surfactant molecules from the disintegrating aggregates to the almost pure surface through a layer of constant thickness, δ, which is of the order of the mean distance between two neighbour aggregates (figure 8). Since the concentration of free surfactant molecules in the neighbourhood of the aggregates is equal to $1\times cac$, the difference between c and c_{sub} is also of the order of $1\times cac$. The flux J can, therefore, be estimated as $J=D\times cac/\delta$, where δ is now equal to the mean distance between two neighbour aggregates.

The leading role of the aggregates disintegration in concentrated solutions is confirmed by the increase of the lamella size for DOS at $10\times cac$ which is not as large as at $1\times cac$ (figures 4,5) while the bulk concentrations of free surfactant monomers, $c=1\times cac$, are the same in both solutions.

Below, we only consider a theoretical model for highly concentrated solutions in which surfactant effects are more significant. In this case, δ=const and the combination $D\times cac/\delta$ is everywhere constant. A model for dilute solutions could be similarly considered assuming that $\delta\sim rPe^{-1/2}$.

4.3. Constitutive equations

Integrating equation (5) with $J=D\times cac/\delta$ and using the boundary conditions $r=r_s$, $v=v_s$, $\Gamma=\Gamma_s$, we obtain the surfactant distribution in the lamella surface:

$$\Gamma\left(r\right)vr = \Gamma_S v_S r_S + \frac{D\times cac}{2\delta}\left(r^2 - r_S^2\right) \qquad (7)$$

Locally, the surface concentration Γ is related to γ by the asymptotic form of the Langmuir-Frumkin equation of state

$$\gamma(r)-\gamma_w=-RT\Gamma(r), \text{ with } \Gamma/\Gamma_\infty\ll1 \qquad (8)$$

where R is the gas constant and T the temperature.

Introducing (8) in (7), we obtain the dependence of γ with r as

$$\gamma\left(r\right) = \gamma_w - \left(\gamma_w - \gamma_s\right)\frac{v_S r_S}{vr} - \frac{D\times cac}{2\delta}\left(r^2 - r_S^2\right)\frac{RT}{vr} \qquad (9)$$

where $v=v(r)$ is the velocity distribution in the lamella.

In this work, we are mainly interested by the influence of the surfactants and dynamic surface tension effect on the maximum size of the lamella. To simplify the physical problem, we assume that due to the fast deformation of the

lamella surface the local surface tension γ is far from equilibrium $1-\gamma/\gamma_w \ll 1$, and that J is the main restoring flux, neglecting by residual surfactant. Due to the last approximation we can suppose for simplicity $r_s = 0$.

By substituting (9) into (4) with $\gamma_s = \gamma_w$, we obtain the equation of the sheet motion in dimensionless form as

$$\left(1 - \frac{FX^2}{V^2}\right)\frac{dV}{dX} = -\frac{FX}{V} \tag{10}$$

where $X = r/r_m^w$, $V = v/v_s$, $r_m^w \equiv \rho q_s v_s / 4\pi\gamma_w$ is the maximum radius of steady water lamella [8] and

$$F = RT \frac{D \times cac}{\delta} \frac{r_m^w}{2\gamma_w v_s} .$$

The boundary condition is
$$V = 1 \text{ at } X = 0. \tag{11}$$

The analytical solution of (10) is obtained as

$$X = \sqrt{-\frac{2V^2}{F}\ln V} . \tag{12}$$

The dimensionless form of the distribution of surface tension $\Sigma \equiv \gamma/\gamma_w$ in the lamella is

$$\Sigma = 1 - \frac{FX}{V} . \tag{13}$$

The distribution of the local Weber number in the lamella $We \equiv \rho h v^2 / 2\gamma = V/\Sigma X$ is determined if both $V = V(X)$ and $\Sigma = \Sigma(X)$ are known. The condition $We = 1$ that defines the position X_m of the free rim of the steady lamella follows from (1). It writes:

$$We = \frac{V_m}{\Sigma_m X_m} = 1 \tag{14}$$

where index "m" indicates the values near the free rim.

4.4. Effect of the surfactant flux

The solution $V(X)$ of (12), and the surface tension distributions (13) are plotted in figures 9 and 10 for different values of the parameter F which measures the effect of the surfactant flux from the bulk to the surface. Only parts of the curves up to the points of return satisfy the boundary conditions, and therefore only these parts are appropriate from a physical point of view. They are drawn in black. These plots show that due to the surfactant flux, the surface tension gradient is negative, which causes a deceleration of the flow in the lamella. This effect increases as F increases.

The common feature to all curves is that a steady flow exists only up to a certain critical point $X_*(F)$ beyond which it becomes impossible. At the critical point, $dV/dX = d\Sigma/dX = -\infty$. Introducing $dX/dV = 0$ in (12), we obtain the values of the critical velocity V_* and of X_* as $V_* = \exp(-1/2) = 0.60653$ and $X_* = 0.60653/F^{1/2}$: V_* does not depend on F, whereas X_* decreases as F increases. The finite values of the velocity and of the thickness at the critical point mean that the flow continues beyond the critical point X_*, but it becomes unsteady or/and it loses its spatial uniformity): $v = v(r,t,\chi)$, $h = h(r,t,\chi)$, where χ is additional coordinate - the polar angle in cylindrical

coordinate system. In other words, X_* is the F-dependent position of the boundary between steady uniform and unsteady (or/and non-uniform) flow in the lamella. We do not know now which kind of flow is formed at $X > X_*$: regular oscillations, regular spatial waves, chaotic instability, turbulence or anything else? It is only obvious that this temporal or/and spatial instability can have a great influence on the lamella dynamics.
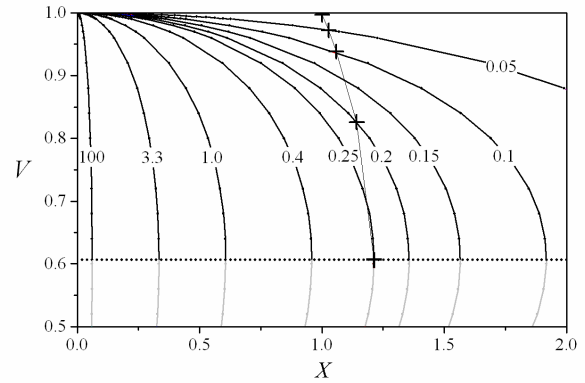
Fig. 9: Effect of surfactant flux on the radial distribution of velocity V for different values of F (indicated on the corresponding curves). The horizontal dotted line represents the critical level $V_* = 0.60653$. Symbols (+) show the positions of the liquid rim for different values of F.
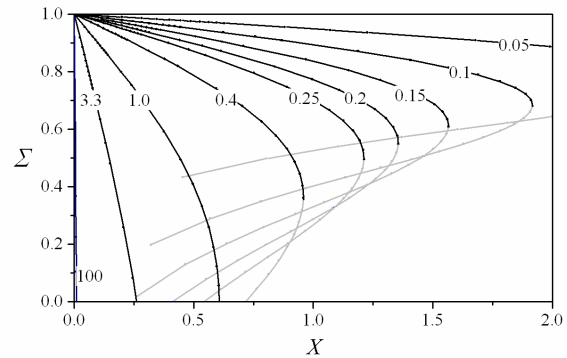
Fig. 10: Effect of surfactant flux on the radial distribution of the surface tension Σ for different values of F (indicated on the corresponding curves).

The maximum size of a steady free lamella X_m is defined by equation (14), which has the solution

$$V_m = \exp\left(-\frac{\left(1 - \sqrt{1 - 4F}\right)^2}{8F}\right) \tag{15}$$

with $X_m = X_m(V_m)$ defined by relation (12).

The values of X_m and V_m are shown in figure 9 by means of crosses on the corresponding curves. Figure 9 shows that the free lamella rim is located in the steady domain $X_m < X_*$ if $F < 0.25$. Obviously, in this case the surfactant flux J enlarges the maximum size of the lamella in this domain since $X_m > 1$ (figure 9). At $F = 0.25$, X_m reaches a maximum $(X_m)_{max} = 1.213$ and V_m a minimum $(V_m)_{min} = V_* = \exp(-1/2) = 0.60653$; simultaneously, X_* is equal to $(X_m)_{max}$, which means that the lamella rim becomes the

boundary of the steady uniform flow if F=0.25.

It is possible to show that We decreases in the lamella with radial coordinate X, but We cannot reach 1 if F>0.25 because equation (15) has no solution in this case. It means that We>1 everywhere in the domain defined by $X<X_*$ and therefore a steady free rim (defined by We=1) cannot be located in the domain of steady uniform flow. What will be with free lamella rim at F>0.25 is not obvious for us, and the mechanism of the rim formation is unclear in this situation.

Comparing the theoretical results for X_m with our experimental data, one may conclude that the observed increase of the lamella size in the case of DOS, 10×cac up to β_m=6.0 (i.e. X_m= β_m/β_m^w=6.0/5.0=1.20) corresponds to a value of $F\approx0.25$ for which the theory predicts a lamella size X_m=1.213. Note that, as figure 9 shows, the increase of the lamella size up to X_m=1.213 is the maximum possible for steady uniform lamella flow.

The theory predicts no surfactant effect on the lamella size if F<<0.25 (figure 9). Thus a low value of parameter F (F<<0.25) can be attributed for Silwett L77 solutions which form lamellas of same size as the water ones.

4.5. Quantification of the effects of the dynamic surface tension

The constitutive parameter $F=RT(D×cac/\delta)\,r_m^w/(2\gamma_w v_s)$ can be independently estimated analysing data in figure 5 on the dynamic surface tensions measured with a Maximum Bubble Pressure method apparatus. With this method the mechanism of formation of the 'dynamic surface tension' is the same as in our experiment and results from the competition between the flux of surfactant from the bulk to the surface and the decrease of surface concentration of surfactant due to the surface fast dilation. Considering the flow at high rate of surface dilation, we can estimate the balance of surfactants at a deforming surface element S as

$$\frac{d\left(\Gamma S\right)}{dt} \sim SD\frac{cac - c_{sub}}{\delta} \qquad (16)$$

from which the estimation of the surface concentration follows

$$\Gamma \sim D\frac{cac - c_{sub}}{\delta\alpha} \qquad (17)$$

where $\alpha \equiv \dfrac{1}{S}\dfrac{dS}{dt}$ is the surface expansion rate in the maximum bubble pressure method.

Using the Langmuir-Frumkin state equation $\gamma_w-\gamma=-RT\Gamma_\infty ln(1-\Gamma/\Gamma_\infty)$ and the Langmuir isotherm $\Gamma\sim\Gamma_\infty c_{sub}/k$, valid for dilute adsorption (where k is a material constant), we obtain from (17) an approximate formula for the surface tension dependence on α

$$\gamma_W - \gamma = -G_1\, ln\left(1 - \frac{RT\left(D×cac/\delta\right)}{G_1\left(\alpha + G_2\right)}\right), \qquad (18)$$

where $G_1=RT\Gamma_\infty$ and $G_2=kD/\Gamma_\infty\delta$.

Considering the asymptotical case $\gamma\rightarrow\gamma_w$ as $\alpha\rightarrow\infty$,

we obtain from (18) $RT(D×cac/\delta)=\lim_{\alpha\rightarrow\infty}[(\gamma_w-\gamma)\alpha] \equiv [(\gamma_w-\gamma)\alpha]_\infty$. The parameter $[(\gamma_w-\gamma)\alpha]_\infty$ characterises the surfactant adsorption rate on the surface. It can be found by best fitting the experimental points in figure 1 to formula (18). Results for the three liquids are presented by solid lines in figure 1 and also in table 1.

Table 1. Parameters characterizing the adsorption kinetics of the surfactants.

Solution	$[(\gamma_w-\gamma)\alpha]_\infty$ (N/(m·s))	F	r_* at $\tau\in[0, 3]$ (mm)	r_* at $\tau\sim5$ (mm)
DOS, 1×cac	2.48	0.034	22.2	3.3
DOS, 10×cac	65.4	0.901	4.30	0.65
Silwett L77 10×cac	1.6	0.022	27.6	4.1

We can now rewrite F as $F=[(\gamma_w-\gamma)\alpha]_\infty\, r_m^w/(2\gamma_w v_s)$. All quantities defining F are measurable. To compare the theoretical and experimental maximum sizes of the lamella, we put $v_s\sim v_i$=3.4 m/s, γ_w=0.072 N/m, and $r_m^w=\beta_m^w d_i/2$ =5.0×0.0027/2=0.00675 m. The parameters so estimated (table 1) correlate well with the experimental observations of the present work. The values of F, 0.034 for DOS at 1×cac and 0.022 for Silwett L77 at 10×cac predict the absence of effect of the surfactant on the maximum lamella size (figures 3 and 4), as it was indeed observed in the experiments. Besides, estimated value F=0.901 for DOS, 10×cac is in the same order of magnitude as F=0.25, which, according to figure 9, predicts the increase of the lamella size up to the level β_m=6.0 as measured experimentally (figure 5). Therefore, the observed increase of the lamella size of DOS, 10×cac is caused by an adsorption kinetics of the surfactant molecules that is faster in this solution than in the other ones studied in this work.

4.6. Hole nucleation

Let us consider now the spontaneous hole nucleation in the light of our theoretical results. As a first approximation, we can assume the flow in the lamella as sequences of a number of steady flows. The first flow regime corresponds to the growth of the lamella up to its maximum size. The latest flow regime is characterised by a very weak liquid ejection, the existence of the lamella being made possible by the slowing down of the liquid rim retraction due to its high inertia. Massive rim plays the role of 'lamella holder'. Correspondingly, the first and the latest flow regimes are characterised by different values of F and as a consequence by different coordinates of the boundary of the steady uniform flow, r_*.

In dimensional form, the critical coordinate X_*=0.60653/$F^{1/2}$ is written as

$$r* = 0.606\left(\frac{2\gamma_w v_s r_m^w}{\left[\left(\gamma_w - \gamma\right)\alpha\right]_\infty}\right)^{1/2}. \qquad (19)$$

At the initial stage of the lamella existence $\tau \in [0, 3]$ the flow velocity is estimated as $v \sim v_i = 3.4$ m/s, and the equivalent water lamella radius $r_m^w = 6.75$ mm. In this case according to (19) the critical radius r_* has the same order of magnitude or exceeds significantly the current maximum radius of the lamella $r_l \sim r_m^w = 6.75$ mm − see table 1. It means that the flow in the lamella occurs in a domain where a steady uniform flow is possible, $We > 1$ and it continues up to the rim, where $We = 1$.

At the latest stage of the lamella existence ($\tau \sim 5$), another hydrodynamic situation exists. Using our experimental estimations of the kinematic data for the flow at $\tau \sim 5$ in [6] ($h \sim 25$ μm, $v \sim 1$ m/s), the continuity equation (3), and the Taylor formula for the lamella maximum size [8] $r_m^w = \rho q v / 4 \pi \gamma_w$, we obtain $r_m^w \sim 0.5$ mm. The corresponding values of r_* calculated with formula (19) are presented in table 1. Relatively small values of r_* are obtained whereas the lamella size r_l at $\tau \sim 5$ remains large $r_l \sim r_m^w = 6.75$ mm (figure 5), which illustrates well the holder role of the rim. Therefore, we observe a large decrease of r_* from the level $r_* > r_l$ at the early stage of the impact, down to the level $r_* < r_l$ at the latest one (figure 11). It means that a steady uniform flow cannot occur in the part of the lamella at $\tau \sim 5$. We suppose that the transition of the flow to the unsteady or/and spatially non-uniform regime is the main reason of the hole formation.
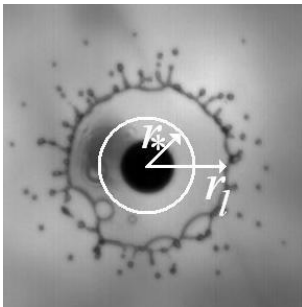
Fig. 11. Image of a lamella displaying the position r_* of the limit between stable ($r < r_*$) and unstable ($r_* < r < r_l$) domains.

However the precise mechanism is still unclear. The unsteady or/and non-uniform character of the flow is not a sufficient condition for hole formation. Experiments with different liquids or even with different drops of a same liquid show that the lamella rupture has a random character. In reality, hole nucleations in the liquid film result from a thickness instability in a region beyond r^* where $We < 1$ and where Marangoni effects cannot restore the uniformity of the thickness.

5. CONCLUSION

Surfactant additives increase the size and the lifetime of the liquid lamella resulting from the impact of drop on a small target because of the fast decrease of the surface tension forces in the case of fast surfactants. They could hinder splashes that generate spider-like liquid structure at the end of the impact. Paradoxically, we could also observe spontaneous nucleation of expanding holes giving to the lamella a web-like structure. The observed holes formation

is likely connected with the coexistence of stable and unstable domains in the lamella generated by surface tension gradients in the latest stage of the experiment. These results may be of great assistance for the choice of additives for the formulation of sprays.

6. REFERENCES

1. Mourougou-Candoni, N., Prunet-Foch, B., Legay, F., Vignes-Adler, M. and Wong, K. Influence of dynamic surface tension on the spreading of surfactant solution droplets impacting onto a low-surface-energy solid substrate, J. Colloid Interface Sci., Vol. 192, pp. 129-141, 1997.

2. Zhang, X. and Basaran, O.A., Dynamic surface tension effects in impact of a drop with a solid surface. J. Colloid Interface Sci. Vol. 187, pp. 166-178, 1997.

3. Mourougou-Candoni, N., Prunet-Foch, B., Legay, F., Vignes-Adler, M. and Wong, K. Retraction phenomena of surfactant solutions drop upon impact on a solid substrate of low surface energy, Langmuir, Vol. 15, pp. 6563-6574, 1999.

4. Svitova, T.F., Smirnova, Yu.P., Pisarev, S.A. and Berezina, N.A. Self-assembly in dilute-tailed surfactants in dilute aqueous solutions Colloids Surf. A Vol. 98, pp. 107-115, 1995.

5. Hill, R.M., He, M., Davis, H.T. and Scriven, L.E., Comparison of the liquid crystal phase behavior of four trisiloxane superwetter surfactants. Langmuir, Vol. 10, pp. 1724-1734, 1994.

6. Rozhkov, A., Prunet-Foch, B. and Vignes-Adler, M. Impact of water drops on small targets. Phys. Fluids Vol. 14, pp. 3485-3501, 2002.

7. Rozhkov, A., Prunet-Foch, B. and Vignes-Adler, M. Impact of drops of polymer solutions on small targets. Phys. Fluids Vol. 15, pp. 2006-2019, 2003.

8. Taylor, G.I. The dynamics of thin sheets of fluid. I. Water bells II. Waves on fluid sheets. III. Disintegration of fluid sheets Proc. R. Soc. Lond. A, Vol. 253, pp. 289-321, 1959.

9. Edwards, D.A., Brenner, H. and Wasan, D.T., Interfacial Transport Processes and Rheology, Butterworth-Heinemann, 1991.

10. Levich, V.G. Physicochemical Hydrodynamics. Prentice-Hall, 1962.

11. Daniel, R.C. and Berg, J.C., A simplified method for predicting the dynamic surface tension of concentrated surfactant solutions, J. Colloid Interface Sci. Vol. 260, pp. 244-249, 2003.

12. Breward, C.J.W., Darton, R.C., Howell, P.D. & Ockendon, J.R. 2001 The effect of surfactants on expanding free surfaces. Chem Eng. Sci. Vol. 56, 2867-2878.